*Int. J. Electrochem. Sci.*, 12 **(2017)** 3336 – 3349, doi: 10.20964/2017.04.14

International Journal of
ELECTROCHEMICAL
SCIENCE
www.electrochemsci.org

# Effect of Immersion Time and Temperature on Corrosion Behaviour of Nanocrystalline Al-Fe-Cr Alloy

*Muneer Baig*[1], , *Hany Rizk Ammar*[2,3], *Asiful Hossain Seikh*[1*], *Mohammad Asif Alam*[1], *Nabeel H. Alharthi*[1,4]

[1]AMI-Center of Excellence for Research in Engineering Material, King Saud University, Riyadh, KSA
[2] Mechanical Engineering Department, College of Engineering, Qassim University, Buraidah, Kingdom of Saudi Arabia
[3] Metallurgical and Materials Engineering Department, Faculty of Petroleum and Mining Engineering, Suez University, Suez, Egypt
[4] Mechanical Engineering Department, College of Engineering, King Saud University, Riyadh, Kingdom of Saudi Arabia
[*]E-mail: aseikh@ksu.edu.sa

*Received:* 4 January 2017 / *Accepted:* 16 February 2017 / *Published:* 12 March 2017

The corrosion behavior of Al-10wt.%Fe-5wt.%Cr nanocrystalline aluminium alloy was studied by cyclic potentiodynamic polarization (CPP) and electrochemical impedance spectroscopy (EIS) methods. The nanocrystalline bulk alloy used in this investigation was fabricated by processed metallic powder via mechanical alloying (MA) technique followed by compaction and sintering in a high frequency induction heat sintering (HFIHS) system. The corrosion behavior of the alloy was tested in a 3.5% NaCl solution for different immersion time and temperatures. The outcomes showed that the developed alloy possess good resistance to uniform corrosion at all temperatures. It is also found that increasing the immersion time, results in moving the corrosion potential ($E_{corr}$) towards a higher negative value that leads to decrease the corrosion current ($j_{corr}$) and consequently increase the corrosion resistance ($R_p$) of the alloy.

**Keywords:** Nanocrystalline aluminium alloy, mechanical alloying, corrosion, polarization, EIS.

## 1. INTRODUCTION

Presently, aluminium alloys have been increasingly used in industries such as automobile, aircraft and defense due to their relatively high specific strength [1-4]. However, the notable decrease in their strength levels when exposed to elevated temperatures limits the use of Al alloys in such applications. Previously, the researchers have focused on improving the mechanical properties and

corrosion resistance of Al alloys independently. Various investigations have been put forward to develop new alloys which have both, the high corrosion resistance and strengths at elevated temperatures simultaneously. However, very few investigations were successful in achieving improvement in corrosion resistance as well as strength. Therefore, significant work is being carried out to fabricate new Al alloys that not only exhibit high strength but also show improvement in its corrosion resistance.

The increase in demand to produce high performance Al alloys led to the path of exploring new technology to process the required product for industries. Various transition metals such as Fe, Cr, Nb, Ti etc can be incorporated into the pure aluminium matrix in order to improve the properties at elevated temperatures [5]. Although, a limited quantity of transition metals can be incorporated in Al matrix, the new technique such as mechanical alloying (MA) can help to increase the miscibility of these alloying elements. It has been reported that the solubility of Fe in Al at room temperature can be increased 150 times (~4.4 at.% ) by using MA [6]. The mechanical alloying process is capable to increase the compatibilities of different transition metals and finally a homogeneous alloy can be produced [7-10]. In the MA process, the homogeneous dispersion of alloying elements in the base metal matrix is influenced by various process parameters such as the processing environment, ball-to-powder weight ratio, milling speed and time [9].

Recent studies shown that strength and corrosion resistance of Al, Al–Fe, Al–Ti, Al–Mn, Al–Mg alloys [5, 11–16] and ferrous alloys [17–19] were considerably improved by synthesizing using MA followed by consolidation. The earlier investigations on sputter deposited Al–M (where M = Fe, Cr, Nb, Ti etc.) alloys showed that their corrosion resistance increased considerably due to the solid solubility extension and the passive film formation [20-23]. There is limitation of solid solubility of these alloying elements in Al (eg, 0.77 wt.% for Cr ) in addition to their difference in melting point. For these two reasons, coarse intermetallics were formed due to the addition of transition elements to Al give rise to pitting corrosion. The recent research findings established that the grain size of second phase particles along with its distribution in Al matrix have considerable influence on the corrosion behavior of the alloy [24–26].

In this study, the corrosion resistant properties of nanocrystalline Al-10wt.% Fe-5wt.%Cr (sintered) alloy developed by MA was investigated by immersing the alloy in 3.5% NaCl solution for different immersion time and temperatures.

## 2. EXPERIMENTAL

### *2.1. Production of ultrafine/nanocrystalline Al-10wt.%Fe-5wt.%Cr sintered alloy*

The starting powders to prepare bulk samples for characterization consist of 99.95% pure Al (with an average particle size of 1µm), 99.95% pure Fe (5µm) and 99.5% pure Cr (4µm). The individual powders were initially mixed in the required proportions to produce a blend of Al-10 wt.%Fe and Al-10 wt.%Fe-5 wt.% Cr along with pure Al powder. These blends were annealed in the vacuum furnace maintained at a temperature of 423K for a hold period of 24 hours to remove the

moisture (degassing) from the starting powders. The process control agent (PCA) used in this investigation was Stearic acid (1 wt.%) and was mixed with the annealed mixture inside the glove box. The mixtures were then transferred into the stainless steel bowls inside the glove box maintained under inert atmosphere (Argon). The bowls were tightly sealed inside the glove box using o-rings to prevent any leaking of atmospheric air into the bowls. The mechanical alloying of the mixtures and the milling of pure Al was carried out for a period of 150 hours. After alloying, the mixtures were transferred into the graphite molds and were subjected to vacuum sintering process in a HFIHS machine. The sintering parameters include; heating rate of 823K/min, sintering temperature of 823K with a hold time of 6 min, while maintaining a pressure of 50 MPa [27].

### *2.2 Characterization using X-Ray Diffraction (XRD)*

The crystallite size of the bulk alloy was measured by means of a Bruker X-ray diffractometer, which operates in θ-θ geometry with a Cu-$K_\alpha$ ($\lambda = 0.154$nm) emitter. The scanning was performed for the 2theta values, ranging from 30 to 70°. This scanning range selected was adequate enough to detect the standard peaks of pure Al. The Scherrer equation was used to calculate the crystallite size of the sintered alloy [28]. It is well known that the initial peaks in the XRD profile relate to the crystallite size while the later peaks relate to the lattice strain introduced during the alloying process. Thus, the initial peak of Al in the XRD profile was used to calculate the crystallite size of the sintered alloy. The crystallite size of Al–10wt.%Fe-5wt.%Cr bulk alloy was estimated to be 33 nm.

### *2.3 SEM characterization of the sintered alloy*

The microstructural characterization of the sintered Al–10wt.%Fe-5wt.%Cr bulk alloy was performed using a field emission scanning electron microscope (FE-SEM). Initially, the sintered samples were mirror polished by using various grit sand papers ranging from 100 to 4000. The final polishing was performed using an emery cloth and colloidal Silica solution, to produce a scratch free surface for SEM investigation.

### *2.4 Sample Preparation*

The working electrode (WE) for the electrochemical experiments was nanocrystalline Al–10wt.%Fe-5wt.%Cr alloy, while the reference (RE) and counter electrode (CE) was chosen to be Ag/AgCl and platinum foil, respectively. One of the faces of WE was soldered by a copper wire, mounted by mixing resin and hardener. After curing, the other face of the electrode was grounded with emery paper ranging from 100 to 1000 grit and then cloth polished with alumina slurries. Then the polished surface was thoroughly washed in water and acetone and finally dried with dry air [27]. Analytic grade sodium chloride and distilled water was used in the preparation of 3.5% NaCl solution.

*2.5 Electrochemical Experiment*

The cyclic potentiodynamic polarization (CPP) and Electrochemical Impedance Spectroscopy (EIS) techniques were used to perform the electrochemical experiments in a Galvanostat/Potentiostat Autolab system. The EIS measurement were carried after exposing the sample (WE) in 3.5% NaCl solution for 1 hour at the open circuit potential ($E_{OC}$) in the 100 kHz ~100 mHz frequency range. The CPP experiments were performed by increasing the potential at the rate of 1.67 mV/s for the scanning range of 1200 to 0.00 mV against RE at open circuit potential (OCP). To complete the cycle, the scanning was performed in opposite direction while maintaining the scanning rate and testing range. For each experiment, freshly polished electrodes were used in a new electrolyte. The experiments were carried out at different immersion time and at different temperatures. The time periods investigated were 0, 1 and 24 hours while the temperatures studied were room temperature (RT), 313 K and 333 K.

## 3. RESULTS AND DISCUSSION

*3.1. Microstructural Characterization*

The SEM micrograph along with Electron Dispersive Spectra (EDS) of nanocrystalline Al–10wt.%Fe-5wt.%Cr bulk alloys are shown in Fig.1. From the figure, it is established that the sintered alloy did not show the presence of porosity on its surface, indicating that the samples produced in this investigation were mostly dense. The experimental density of the alloy measured through the Archimedes principle was found to be 2.97 g/cm$^3$. The EDS analysis performed on the entire SEM micrograph showed the presence of alloying elements, Fe and Cr, in the sintered alloy.

The XRD peaks for the sintered Al-10wt.%Fe-5wt.%Cr alloy, produced in this investigation is shown in the Fig. 2. From the figure it is observed that the recorded peaks correspond to the (111), (200) and (220) planes of Al. Also, from the figure it is noted that the presence of the alloying elements (Iron and Chromium) are not clearly established. However, the results obtained from EDS (shown in Fig. 1) clearly depicted the existence of alloying elements in the sintered sample. Thus, it could be implied that the Fe and Cr formed a supersaturated solid solution (SSS) with Al after 150 hours of mechanical alloying.

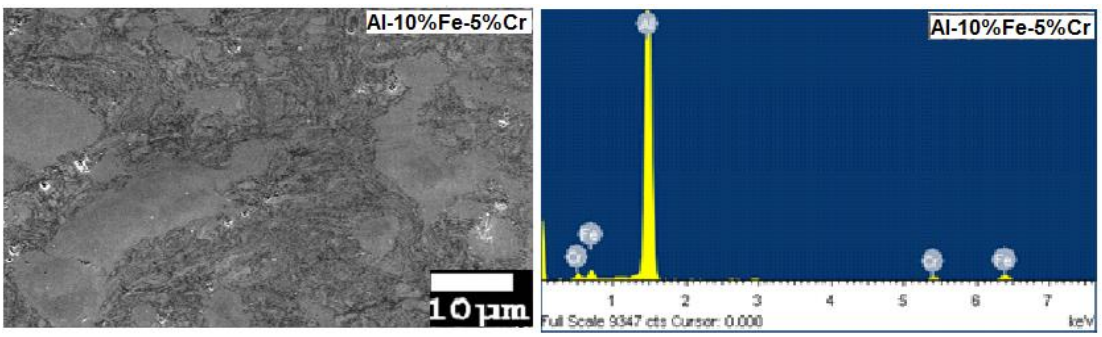


**Figure 1.** SEM micrograph and EDX spectrum analysis obtained on the nanocrystalline Al10Fe5Cr alloy before immersion.

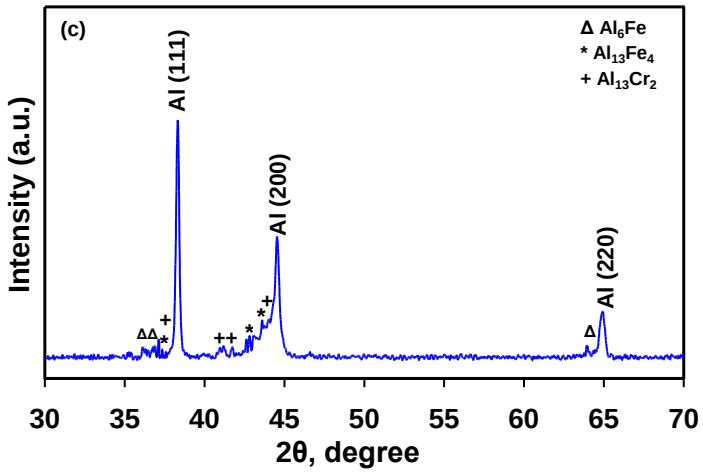


**Figure 2.** XRD analysis obtained on the nanocrystalline Al-10% Fe -5%Cr sintered alloy

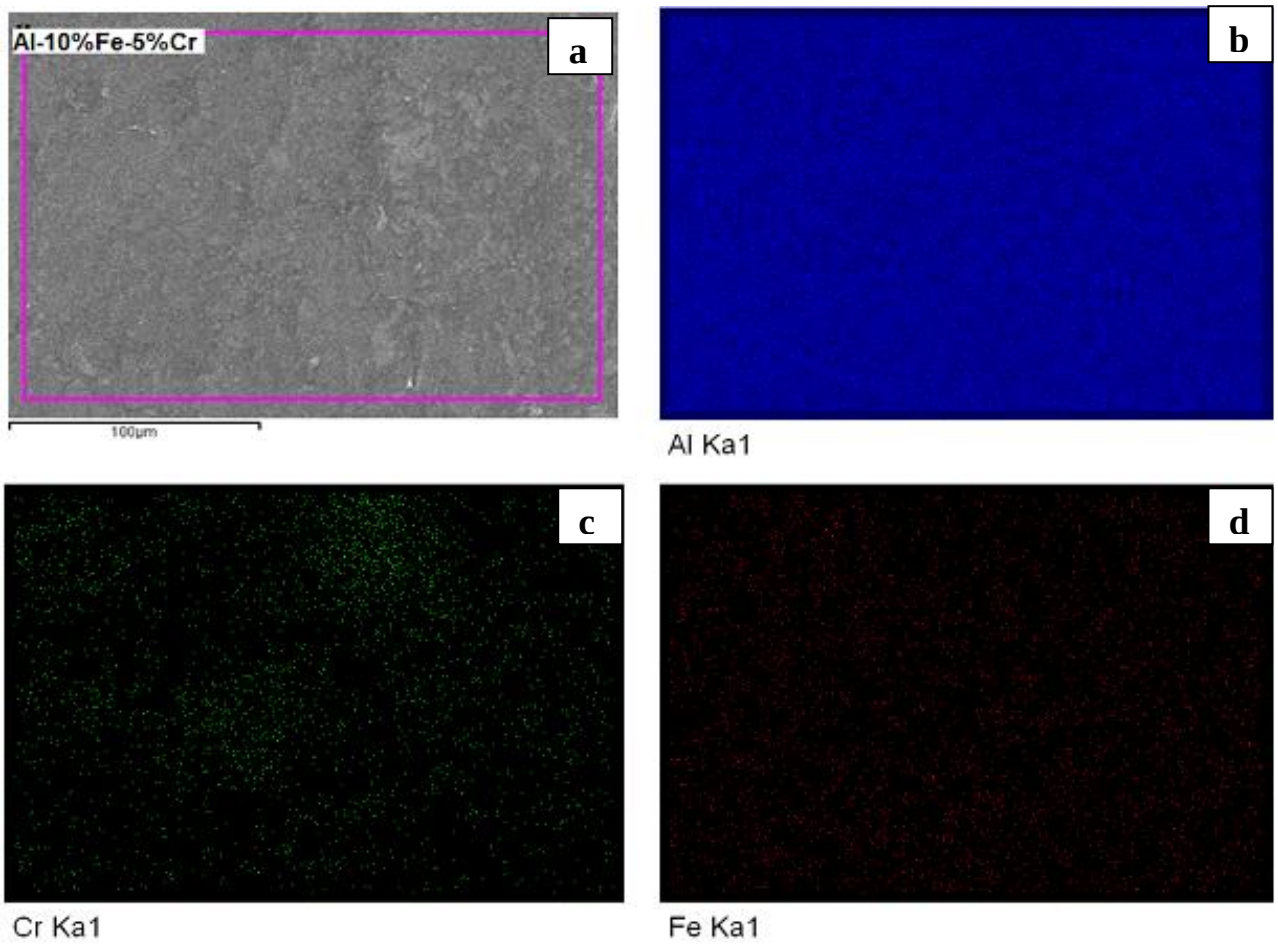


**Figure 3.** Elemental Mapping of (a) Al-10% Fe -5%Cr sintered alloy indicating the presence of (b) Al, (c) Cr and (d) Fe.

However, due to their lower concentrations in the initial mixture and the peak overlapping, the presence of these elements is not confirmed with XRD data. Based on the broadening of the peaks in

the XRD data it is clear that the grain refinement has taken place as a result of mechanical alloying process. Fig. 2 also shows that the sintering process has resulted in the formation of two new phases /or intermetallics $Al_6Fe$, $Al_{13}Fe_4$ and $Al_{13}Cr_2$. The formation of these intermetallics imparts the strength to the sintered alloy. The crystallite size of the bulk alloy was calculated using the initial Al (111) peak and was estimated to be 33 nm using Scherrer equation. The average hardness value of the Al-10wt.%Fe-5wt.%Cr alloy obtained using the Vickers micro-hardness test was found to be 3.4 GPa

Fig.3 shows the electron back scatter images of the Al-10wt.%Fe-5wt.%Cr alloy and the elemental mapping of Cr and Fe in the Al matrix. From the figure, it is clear that the MA performed in this investigation has led to the homogeneous dispersion of Cr and Fe in the Al matrix either in elemental form or intermetallic phases.

*3.2 Polarization Measurements*

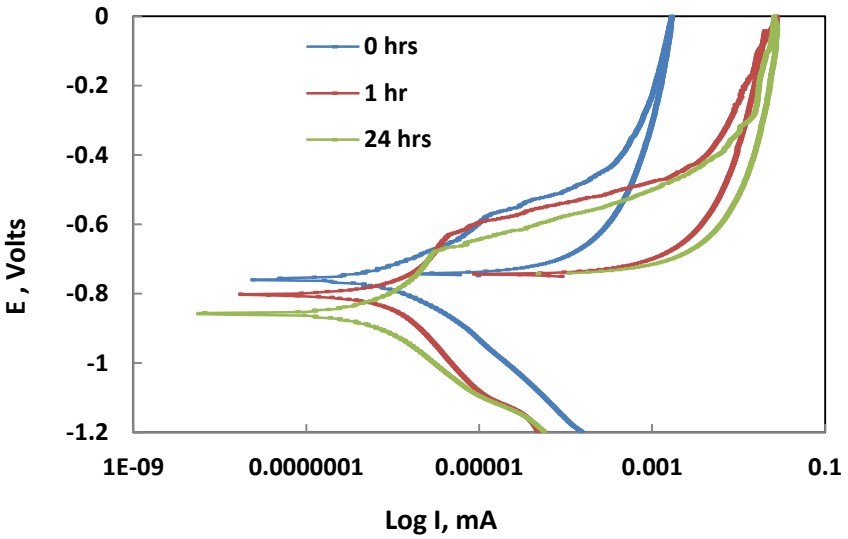


**Figure 4.** Potentiodynamic polarization curves for Al - 10% Fe - 5%Cr alloy in 3.5% NaCl at RT after 0hr, 1 hr and 24 hrs.

**Table 1.** The parameters of Cyclic Potentiodynamic polarization of Al - 10% Fe - 5%Cr alloy in 3.5% NaCl at RT after different immersion time.

| Immersion Time (Hours) | Tafel Data | | | | | | | | Linear Polarization Data |
|---|---|---|---|---|---|---|---|---|---|
| | $\beta_a$ mV/Dec | $\beta_c$ mV/Dec | $E_{corr}$, mV | $J_{corr}$, $\mu Acm^{-2}$ | $E_{pass}$, mV | $J_{pass}$, $\mu Acm^{-2}$ | $E_{pit}$, mV | $J_{pit}$, $\mu Acm^{-2}$ | $R_p$ $k\Omega cm^2$ |
| 0 | 68.71 | 80.94 | -759 | 1.0602 | -648 | 5.11 | -584 | 13.45 | 15.240 |
| 1 | 75.47 | 84.24 | -802 | 0.7955 | -706 | 2.32 | -633 | 4.84 | 21.756 |
| 24 | 78.31 | 86.92 | -856 | 0.4809 | -795 | 0.99 | -675 | 3.39 | 37.244 |

The CPP curves were studied after exposing the sintered alloy in an aerated 3.5% NaCl solution for different immersion time. Fig. 4 shows the CPP curves from which the corrosion parameters were determined. Table 1 shows the values of the cathodic Tafel ($\beta_c$) and anodic Tafel ($\beta_a$) slopes, pitting potential ($E_{Pit}$), passivation current ($j_{Pass}$), passivation potential ($E_{Pass}$), pitting potential ($j_{Pit}$), corrosion current density ($j_{Corr}$), corrosion potential ($E_{Corr}$), and polarization resistance ($R_p$). The corrosion current density, $j_{corr}$, was determined graphically by extrapolating the cathodic and anodic Tafel slopes to the $E_{corr}$ (versus Ag/AgCl). The value of $R_p$ was calculated from the Stern-Geary equation [29]: $R_P = 1/j_{Corr} .[\beta_c . \beta_a/ 2.3 (\beta_c + \beta_a)]$.

From polarization curve, it is observed that the cathodic current of tested alloy moves to less negative value with increasing the potential till the current reaches its minimum at the corrosion current density, $j_{Corr.}$ The cathodic reaction for Al and its alloys is as follow [30]:

$$O_2+2H_2O + 4e^- = 4OH^- \quad (1)$$

When the potential increases towards the positive direction, the current in the anodic reaction increases rapidly as a result of the dissolution of Al as follow [30]:

$$Al=Al^{3+}+3e^- \quad (2)$$

The formation of the passive region in the polarization curve is related to the presence of oxide film on the outer surface of Al and its alloys. The reaction between Al ion and hydroxyl ion forms Aluminium hydroxide layer on the surface:

$$Al^{3+}+3OH^- =Al\ (OH)_{3,\ ads}+3e^- \quad (3)$$

This Aluminium hydroxide further converts to Aluminum oxide as follow:

$$Al\ (OH)_{3,\ ads}=Al_2O_3+H_2O \quad (4)$$

The oxide thus formed prevents the Al surface against corrosion by forming passive layer up to breakdown potential. Further increase in potential, abruptly increases current resulting in breakdown passive layer which initiates pitting corrosion [30]. Following the degradation of passive layer, the chloride ions from the solution attacks the Al surface resulting in the formation of Aluminum chloride complex ($AlCl_4$) by the following reaction:

$$Al^{3+} + 4Cl^- = AlCl_4 \quad (5)$$

The formation of $AlCl_4$ leads to the development of pitting corrosion which is clearly displayed by the presence of wide hysteresis loop.

From the polarization diagram, $J_{corr}$ values were estimated by extrapolating anodic and cathodic Tafel slopes to the $E_{corr}$. It is observed from Fig. 4 that as the immersion time increases, the values of anodic and cathodic currents, $j_{Corr}$, $j_{Pass}$, $j_{Pit}$ decreases and the $\beta_c$, $E_{Corr}$, $E_{Pass}$ and $E_{Pit}$ values are shifted to the more negative direction. From Table 1 it is also confirmed that with immersion time, the polarization resistance ($R_p$) increases. Therefore, it is concluded from the results that the rate of corrosion in the sintered alloy decreases as the time of immersion increases. It is also evident from Table 1 that a high value of polarization resistance ($R_p$) is achieved at all immersion conditions. This enhancement in the polarization resistance could be due to the microstructural stability and the passive layer formation of metal oxides as shown in XRD analysis in Fig. 9. This is in agreement with the work by Frangini et. al [31] who also reported that the alloying elements Cr or Ti increases the protection by suppressing the impassiveness of the Aluminium oxide film.

The addition of Cr to Al-10%Fe alloy favored the increase in $R_p$ with increasing immersion time as Cr enhances the strength of Aluminum oxide deposit.

### *3.3 EIS Studies*

To compare the results obtained from polarization, mechanical and kinetic parameters of the alloy was investigated by EIS experiment. Figure 5 shows the Nyquist plot of the sintered alloy at different exposure times. An equivalent circuit used to analyze the experimental results from the Nyquist plots is shown in Fig.6. Table 2 shows the values of solution resistance ($R_s$), the charge transfer resistance ($R_{ct}$), Rf is the film resistance and $C_f$ is the capacitance value obtained using the equivalent circuit [32]. In order to get perfect fit, the substitution of Constant phase elements (CPEs) is correlated by the double-layer capacitance ($CPE_{dl}$ or $C_{dl}$) and the pseudo-capacitance ($CPE_f$ or $C_f$) for the capacitive elements. The alloy corrosion resistance is determined by the parameter $R_{ct}$ which is inversely proportional to corrosion current density $j_{corr}$.

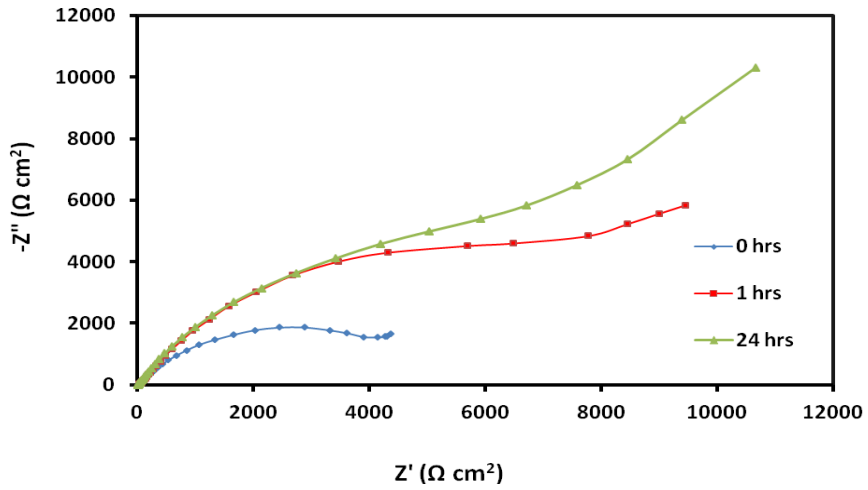


**Figure 5.** Nyquist plot of Al-10% Fe-5%Cr alloy in 3.5% NaCl at RT for 0, 1, and 24 hrs of immersion.

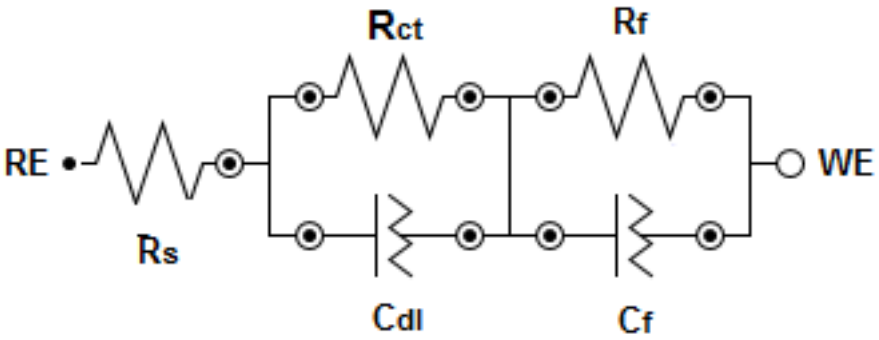


**Figure 6.** Equivalent circuit fitting for EIS.

**Table 2.** Parameters of Electrochemical Impedance of Al - 10% Fe - 5%Cr alloy in 3.5% NaCl at RT after 0 hr, 1 hr and 24 hrs immersions.

| Exposure period | Kinetic EIS parameters | | | | | | |
|---|---|---|---|---|---|---|---|
| | $R_S$ / Ω $cm^2$ | $CPE_{dl}$ | | $R_{ct}$ / kΩ $cm^2$ | $CPE_f$ | | $R_f$ / kΩ $cm^2$ |
| | | $Yc_{dl}$/μMho $cm^{-2}$ | n | | $Yc_f$/ μMho $cm^{-2}$ | n | |
| 0 hour | 8.38 | 55.1 | 0.978 | 5.2 | 920 | 0.61 | 13.6 |
| 1 hour | 5.36 | 48.1 | 0.999 | 7.05 | 363 | 0.54 | 17.1 |
| 24 hour | 7.38 | 35 | 0.962 | 11.2 | 192 | 0.51 | 36.6 |

The Nyquist diagram for 0 hr, 1 hr and 24 hrs of immersion time shows two semicircles at lower and higher frequencies which are capacitive in nature. The semicircle at a higher frequency is attributed to the charge-transfer reaction from the alloy to the solution. On the other hand, the semicircle at low frequency is attributed to the development of passive layers, probably oxides of Al, Fe and Cr, or corrosion products as evident from CPP curves shown in Fig.4.

It has also been observed from the Nyquist plot that with increasing immersion time the width of the semicircle is considerably increased. The values of both $R_{ct}$ and $R_f$ enhanced with longer time of immersion as shown in Table 2. The higher values of $R_{ct}$ suggest that the corrosion resistance of the alloy is enhanced possibly due to the formation of stable oxide formation [33]. Therefore, the experimental outcomes from EIS results are in agreement with the potentiodynamic polarization results.

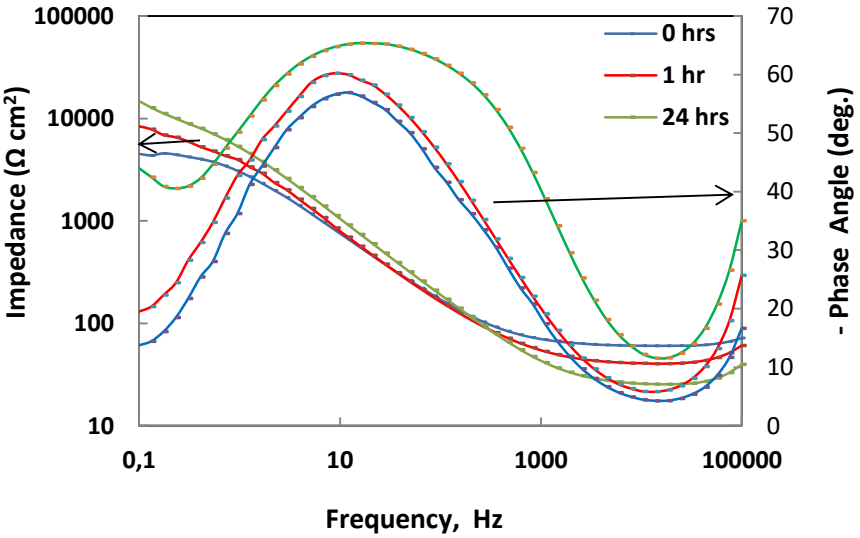


**Figure 7.** Bode plot of Al - 10% Fe - 5%Cr alloy in 3.5% NaCl at RT after 0hr, 1hr and 24 hrs immersions.

Bode-phase plots were evaluated from impedance data to investigate the surface of the sample during the impedance measurement. The Bode-phase diagram for Al-10wt.%Fe-5wt.%Cr ternary (sintered) alloy is shown in Fig.7. From the figure, the total value of impedance of the sintered alloy

was found to be 4.6kΩ $cm^2$ after immediate exposure in NaCl solution. This shows the improvement in corrosion resistance of the alloy. Similarly, the total impedance value of sample after 24 hrs immersion was found to be 14.2kΩ $cm^2$. The impedance values obtained during the experiments clearly indicate that the alloy corrosion resistance increases with immersion time.

On the other hand, Bode-phase diagram showed two time constants, depicting highly corrosion resistance capacity which is a typical property of all passive materials. The approach of phase angle to -70° is ultimately due to low to medium frequency which suggested a very stable film formation on the surface of the sintered alloy.

*3.4 Microstructural characterization of the sintered alloy after corrosion*

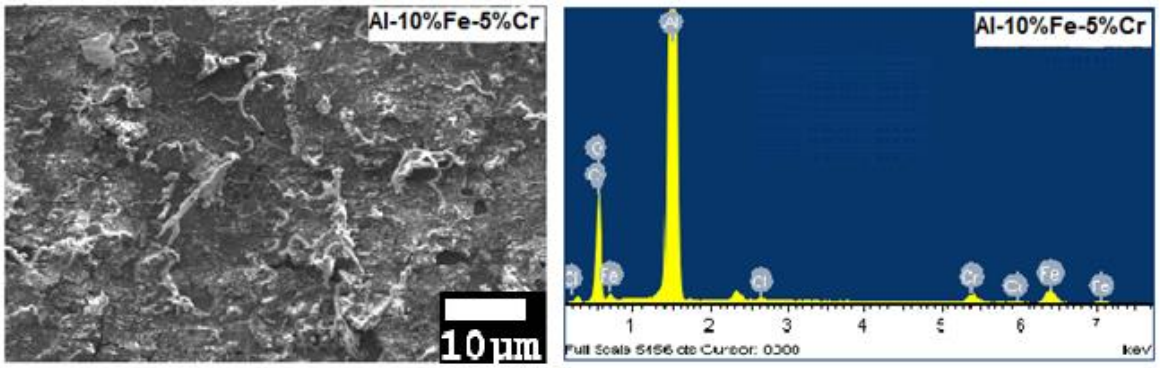


**Figure 8.** SEM image and EDX spectrum obtained on the nanocrystalline Al - 10% Fe - 5% Cr alloys after immersion in 3.5% NaCl for 24 hr.

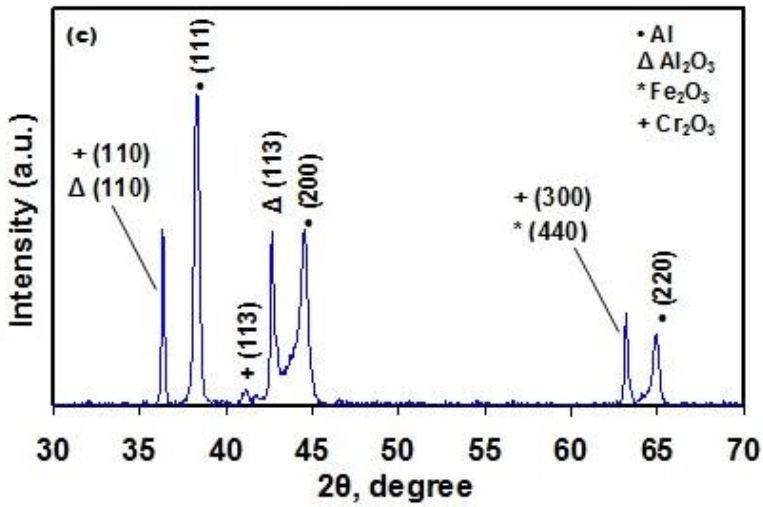


**Figure 9.** XRD pattern attained on the nanocrystalline Al - 10% Fe - 5%Cr alloy after corrosion.

Fig.8 shows the SEM micrograph of the sintered alloy after corrosion, along with its corresponding EDX spectrum. The results from the EDX clearly indicate the presence of Oxygen in the SEM micrograph. The existence of oxygen in the EDX spectrum is related to the passive layer

formation which contains oxides of Al, Fe and Cr on the alloy surface. An elemental investigation on the corroded sample showed the presence of (in weight percentages) 30.01%O, 61.05%Al, 1.65%Cl, 5.26%Fe and 2.03%Cr on the alloy surface. On the contrary, the EDX examination of this alloy before corrosion showed (in weight percentages) 84.71%Al, 10.09%Fe and 5.2%Cr on its surface. Thus, it is clear that the weight percent of Al decreased after exposure to corrosion. This may be attributed due to the dissociation of Al in NaCl solution [34-35].

Moreover, the existence of oxygen in corroded alloy obviously shows the development of oxidation on the surface. The SEM micrograph in Fig. 8 shows coarse and denser surface layer formed by the corrosion products of Cl, O, Al, Fe and Cr. According to the EDX analysis of the corroded sample, the weight percent of the elements Al, Fe, Cr decreases and weight percent of O and Cl increases. This is due to the existence of a passive layer on the surface of Al alloy formed by the products of corrosion [36-37]. The corrosion product in the passive layer was mostly $Al_2O_3$ due to the existence of high weight percentages of O and Al and low weight percentages of Fe and Cr oxides. The XRD pattern in Fig. 9 clearly shows the presence of oxides due to the degradation of the outer surface of the sintered alloy. The XRD results also support the SEM/EDX analysis as both shows the presence of oxygen (oxide) after exposure.

### *3.5 Effect of Temperature*

To study the temperature effect on the corrosion behavior, the electrochemical tests were accomplished on the sintered alloy at higher temperatures in 3.5% NaCl solution. Fig. 10 shows the cyclic polarization curves for the sintered alloy after exposure to 3.5% NaCl solution for 60 min at RT, 313 K and 333 K. The corrosion variables that were calculated from the obtained polarization curves are shown in Table 3.

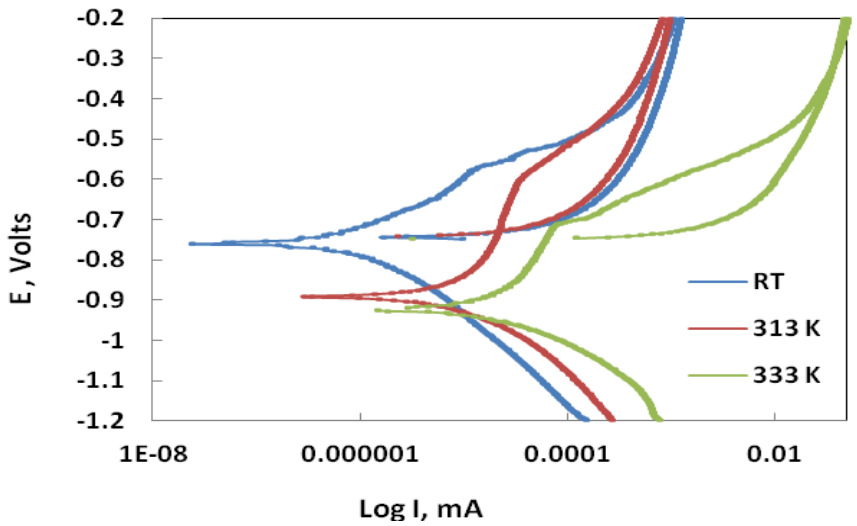


**Figure 10.** Cyclic potentiodynamic polarization curves for Al - 10% Fe - 5%Cr alloy in 3.5% NaCl at RT, 313 K, and 333 K.

**Table 3.** Potentiodynamic polarization parameters of Al - 10% Fe - 5%Cr alloy in 3.5% NaCl at RT, 313 K and 333 K.

| Solution Temperature | Tafel Data | | | | | | | | Linear Polarization Data |
|---|---|---|---|---|---|---|---|---|---|
| | $\beta_a$ V/Dec | $\beta_c$ V/Dec | $E_{corr}$, mV | $J_{corr}$, $\mu Acm^{-2}$ | $E_{pass}$, mV | $J_{pass}$, $\mu Acm^{-2}$ | $E_{pit}$, mV | $J_{pit}$, $\mu Acm^{-2}$ | $R_p$ $k\Omega cm^2$ |
| RT | 68.71 | 80.94 | -759 | 1.0602 | -648 | 5.11 | -584 | 13.45 | 15.240 |
| 313 K | 85.54 | 94.92 | -891 | 5.04 | -743 | 20.07 | -607 | 32.62 | 3. 881 |
| 333 K | 88.26 | 98.34 | -915 | 14.35 | -808 | 43.88 | -709 | 82.15 | 1.409 |

From Table 3, it is confirmed that corrosion density is high and the polarization resistance is low at higher temperature. This is due to the increase in temperature the surface activation increases and thus corrosion rate increases due to dissolution [38].

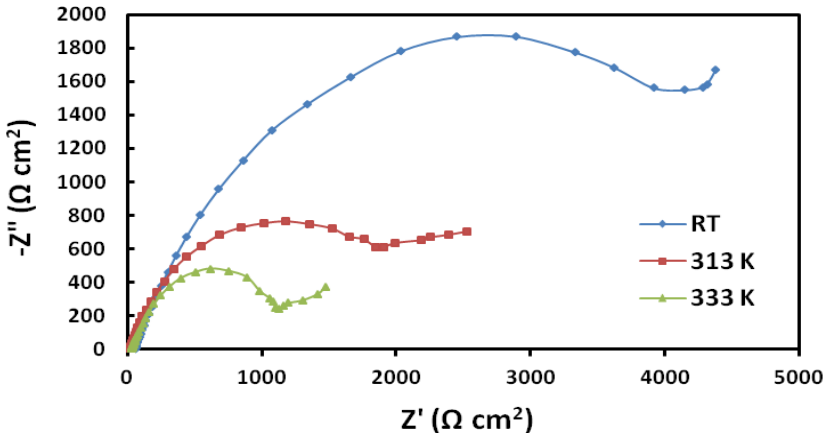


**Figure 11.** Nyquist plot of nanocrystalline Al - 10% Fe - 5%Cr alloy in 3.5% NaCl at RT, 313 K and 333 K.

**Table 4**. Electrochemical Impedance parameters of Al - 10% Fe - 5%Cr alloy in 3.5% NaCl at RT, 313 K and 333 K.

| Solution Temperature | Kinetic EIS parameters | | | | | | |
|---|---|---|---|---|---|---|---|
| | $R_S$ / $\Omega$ $cm^2$ | $CPE_{dl}$ | | $R_{ct}$ / $k\Omega$ $cm^2$ | $CPE_f$ | | $R_f$ / $k\Omega$ $cm^2$ |
| | | $Yc_{dl}$/$\mu$Mho $cm^{-2}$ | n | | $Yc_f$/ $\mu$Mho $cm^{-2}$ | n | |
| RT | 8.38 | 55.1 | 0.978 | 5.2 | 920 | 0.61 | 13.6 |
| 313 K | 5.32 | 68.2 | 0.746 | 2.3 | 3134 | 1 | 9.6 |
| 333 K | 4.84 | 75.9 | 0.818 | 1.2 | 5386 | 1 | 2.6 |

Hence, it can be concluded that the rate of corrosion of the alloy increases with solution temperature. It is observed that the polarization resistance ($R_p$) obtained at the highest testing temperature is largest (of the order of $k\Omega cm^2$) in 3.5 wt% NaCl solution. Thus, it may be concluded that the sintered alloy exhibited a higher resistance to corrosion, since Cr improves the protectiveness of aluminum oxide layer.

The Nyquist plot at higher temperatures shows that the curve data is same as that at room temperature. The diameter of the semicircle remarkably decreased at higher temperature as shown in Figure 11. The data in Table 4 shows that with increase in temperature the values of $R_{ct}$ decreases. It is also observed from Figure 11 that the arc diameter exceeds $2k\Omega.cm^2$ indicating the existence of an oxide layer on the outer surface of the sintered alloy. The oxide layer formed shields the alloy from the corrosion atmosphere and improves its resistance to corrosion.

## 4. CONCLUSIONS

In this investigation, bulk nanocrystalline Al - 10wt.%Fe - 5wt.%Cr alloy was produced from mechanically alloyed powders. The starting powder mixture was milled for 150 hours in a planetary ball mill. The MA was performed in a protected atmosphere at room temperature. The MA powders were compacted and sintered in a HFIHS machine to produce the bulk sintered samples. The electrochemical behavior of sintered alloy was studied in 3.5% NaCl solution at various immersion time and temperatures using EIS and CPP techniques. The results showed that the processed nanocrystalline Al alloy exhibited excellent corrosion resistance both at room and high temperatures. Also, it is concluded that increasing the time of immersion in NaCl solution resulted in a significant enhancement in the corrosion resistance of the developed alloy.

ACKNOWLEDGEMENT
This work was funded by the National Plan for Science, Technology and Innovation (MAARIFAH), King Abdulaziz City for Science and Technology, Kingdom of Saudi Arabia, Award number 12-NAN-2635-02.

## References

1. J. Hirsch, *Mater. Trans*., 52 (2011) 818–824.
2. S. Toros, F. Ozturk, I. Kacar, *J. Mater. Process. Technol*., 207 (2008) 1–12.
3. J. R. Davis, ASM speciality Book, 1996.
4. I. J. Polmear, Light Alloys, 4th ed. Butterworth-Heinemann, London; 2006.
5. T. Sasaki, T. Mukai, and K. Hono, *Scr. Mater.*, 57 (2007) 189-192.
6. D. K. Mukhopadhyay, C. Suryanarayana, F.H. Froes, *Metall. Mater. Trans*. A, 26 (1995) 1939–1946.
7. L. Lu, Y.Zhangm, *J. Alloys Compd*., 290 (1999) 279-283.
8. R. Mishra, R. Balasubramaniam, *Corr. Sci*., 46 (2004) 3019-3029.
9. W. Luo, Y Xu, Q. Wang, P.Shi, M. Yan, *Corr. Sci*., 52 (2010) 3509-3513.
10. S. H. Kim, K. T. Aust, U. Erb, F. Gonzalez, G. Palumbo, *Scr. Mater*., 48 (2003) 1379-1384.

11. T. T. Sasaki, T. Ohkubo, K. Hono, *Acta Mater*., 57 (2009) 3529–3538.
12. J.R. Ryu, K. I. Moon, K. S. Lee, *J. Alloys Compd*., 296 (2000) 157–165.
13. V. L. Tellkamp, A. Melmed, E. J. Lavernia, *Metall. Mater. Trans*. A., 32 (2001) 2335–2343.
14. D. Witkin, Z. Lee, R. Rodriguez, S. Nutt, E. Lavernia, *Scr. Mater*., 49 (2003) 297-302.
15. K. M. Youssef, R. O. Scattergood, K. L. Murty, C. C. Koch, *Scr. Mater*., 54 (2006) 251–256.
16. K. A. Darling, A. J. Roberts, L. Armstrong, D. Kapoor, M.A. Tschopp, L.J. Kecskes, S.N. Mathaudu,*Mater. Sci. Eng*. A., 589 (2013) 57–65.
17. R. K. Gupta, K. S. Darling, R.S. Raman, K.R. Ravi, C.C. Koch, B.S. Murthy, *J. Mater. Sci*. 47 (2012) 1562–1566.
18. R. K. Gupta, R. S. Raman, C. J. Koch, *Mater. Sci*., 47 (2012) 6118-6124.
19. R. K. Gupta, N. Birbilis, *Corros. Sci*., 92 (2015) 1–15.
20. G. S. Frankel, M. A. Russak, C. V. Jahnes, M. Mirzamaani, V.A. Brusic, *J. Electrochem. Soc*., 136 (1989) 1243–1244.
21. G. D. Davis, B. A. Shaw, B. J. Rees, M. Ferry, *J. Electrochem. Soc*., 140 (1993) 951–959.
22. J. Creus, A. Billard, F. Sanchette, *Thin Solid Films*., 466 (2004) 1–9.
23. G. S. Frankel, R. C. Newman, C. V. Jahnes, M. A. Russak, *J. Electrochem. Soc*., 140 (1993) 2192–2197.
24. M. Mehmood, E. Akiyama, H. Habazaki, A. Kawashima, K. Asami, K. Hashimoto, *Corros. Sci*., 41 (1999) 477–499.
25. R. A. Bley, J. R. Scully, J. W. P. Hsu, Philos. *Mag. Lett*., 80 (2000) 85–94.
26. R. K. Gupta, A. Deschamps, M. K. Cavanaugh, S. P. Lynch, N. Birbilis, *J. Electrochem. Soc*., 159 (2012) C492–C502.
27. A. H. Seikh, M. Baig, H. R. Ammar, *Int. J. Electrochem. Sci*. 10 (2015) 3054-3064
28. A. Patterson, *Phys. Rev*., 56 (1939) 978.
29. P. R. Roberge, Handbook of Corrosion Engineering; McGrow-Hill: New York, NY, USA, 2000
30. E. M. Sherif, S. M. Park, *Electrochim. Acta*., 51 (2006) 1313–1321.
31. S. Frangini, A. Masci, *Surf. Coat. Technol*., 184 (2004) 3.
32. H. Ma, S. Chen, L. Niu, S. Zhao, S. Li, D. Li, *J. Appl. Electrochem.*, 32 (2002) 65.
33. A. H. Seikh, M. Baig, H. R. Ammar, *Int. J. Electrochem. Sci*., 19 (2015) 3054 - 3064.
34. M. Saxena, O. P. Modi, A. H. Yegneswaran, P. K. Rohatgi, *Corros. Sci*., 27 (1987) 249-256.
35. J. W. Diggle, T. C. Downie, C. Goulding, *Electrochim. Acta*, 15 (1970) 1079–1093.
36. F. D. Wall, M. A. Martinez, J. J. Vandenavyle, *J. Electrochem. Soc.*, 151 (2004) 354–358.
37. S. S. A. Rehim, H. H. Hassan, M. A. Amin, *Appl. Surf. Sci*., 187 (2002) 279–290.
38. E. A. H. A. Zubaidy, F. S. Mohammad, G. Bassioni, *Int. J. Electrochem. Sci*., 6 (2011) 6424–6441.